Decreasing fire season precipitation increased recent western US forest wildfire activity

Zachary A. Holden[a,1], Alan Swanson[b], Charles H. Luce[c], W. Matt Jolly[d], Marco Maneta[e], Jared W. Oyler[f], Dyer A. Warren[b], Russell Parsons[d], and David Affleck[g]

[a]US Forest Service Region 1, Missoula, MT 59807; [b]School of Public and Community Health Sciences, University of Montana, Missoula, MT 59812; [c]US Forest Service Aquatic Science Laboratory, Rocky Mountain Research Station, Boise, ID 83702; [d]US Forest Service, Fire Sciences Laboratory, Rocky Mountain Research Station, Missoula, MT 59808; [e]Department of Geosciences, University of Montana, Missoula, MT 59812; [f]Earth and Environmental Systems Institute, Pennsylvania State University, University Park, PA 16802; and [g]Department of Forestry and Conservation, University of Montana, Missoula, MT 59812

Edited by James T. Randerson, University of California, Irvine, CA, and approved July 23, 2018 (received for review February 7, 2018)

Western United States wildfire increases have been generally attributed to warming temperatures, either through effects on winter snowpack or summer evaporation. However, near-surface air temperature and evaporative demand are strongly influenced by moisture availability and these interactions and their role in regulating fire activity have never been fully explored. Here we show that previously unnoted declines in summer precipitation from 1979 to 2016 across 31–45% of the forested areas in the western United States are strongly associated with burned area variations. The number of wetting rain days (WRD; days with precipitation ≥2.54 mm) during the fire season partially regulated the temperature and subsequent vapor pressure deficit (VPD) previously implicated as a primary driver of annual wildfire area burned. We use path analysis to decompose the relative influence of declining snowpack, rising temperatures, and declining precipitation on observed fire activity increases. After accounting for interactions, the net effect of WRD anomalies on wildfire area burned was more than 2.5 times greater than the net effect of VPD, and both the WRD and VPD effects were substantially greater than the influence of winter snowpack. These results suggest that precipitation during the fire season exerts the strongest control on burned area either directly through its wetting effects or indirectly through feedbacks to VPD. If these trends persist, decreases in summer precipitation and the associated summertime aridity increases would lead to more burned area across the western United States with far-reaching ecological and socioeconomic impacts.

wildfire | climate change | hydrology

The iconic wildfires of 1988 in Yellowstone National Park were notable in their own right, but they also signaled the beginning of a three-decade-long upturn in wildfire activity in the western United States (1–3). Despite many studies showing links between summer precipitation and wildfires (4–7), investigators studying the drivers of increased fire activity have suggested that warming temperatures are the primary culprit, driving earlier snowpack loss leading to longer fire seasons (1) and hotter summer temperatures that dry out woody fuels (8–10). Parallel trends in warming temperatures, declining snowpack, and increasing fire activity certainly support the role of temperature as a driver of wildfire activity, but it is important to check other potential hypotheses. In particular, it is worthwhile to note that the winter of 1988 was about 5 °C colder than normal in Yellowstone, with a near-normal snowpack at the end of the winter, but precipitation all but stopped in May of 1988 for the remainder of the summer. Once again, in 2017, a cold winter and deep snowpack in the northwest United States transitioned into a major fire season on the heels of a dry summer with record-breaking dry spells without wetting rain. These are anecdotal observations, but enough to warrant further exploration of the mechanisms underlying recent trends in wildfire activity.

The importance of winter snowpack for regulating western US fire activity is the most commonly cited hypothesis on how hydrology regulates fire processes (1), even leading to early season forecasts based on spring snow and streamflow conditions. A similarly compelling story has implicated increased surface air temperature, and consequently vapor pressure deficit (VPD), as a driver of fuel moisture and recent wildfire activity (8–10), which supports partial attribution of the increased fire activity to anthropogenic climate change (11). At the same time, there is clear knowledge that summer rain affects fires (4–7), but a lack of testing for its participation in historical wildfire trends. While knowledge about temperature trends and their impacts on wildfire activity is important as a direct link to understanding potential climate change effects, treating the temperature effects in isolation ignores the potential hydrologic feedbacks that are driven by summer moisture variations and could lead to errors in projection and potential maladaptation. In particular, projections of changes in summer precipitation, snowpack, and summer air temperatures have different spatial patterns across regions and elevations, and meaningful use of climate projections can only occur if we can accurately link the different climate elements to fire.

Here we contrast what are now three hypothesized climatic drivers of recent increases in western US wildfire activity: decreased snowpack, increased temperature, and decreased precipitation. Using satellite-derived maps of forest wildfire area burned from eight western US ecoregions (12) (Fig. 1) and daily

Significance

Wildfires have profound impacts on forested ecosystems and rural communities. Increases in area burned by wildfires in the western United States have been widely attributed to reduced winter snowpack or increased summer temperatures. Trends in precipitation have previously been dismissed as has their feedback to regional temperature trends. We show that declines in summer precipitation and wetting rain days have likely been a primary driver of increases in wildfire area burned. Understanding the climatic drivers of fire activity is important for informing forest management. Our findings are consistent with future climate projections, which predict further decreases in summer precipitation and longer dry periods between rain events across much of the West.

Author contributions: Z.A.H., A.S., C.H.L., W.M.J., and M.M. designed research; Z.A.H., A.S., C.H.L., W.M.J., J.W.O., D.A.W., and D.A. analyzed data; and Z.A.H., A.S., C.H.L., W.M.J., M.M., R.P., and D.A. wrote the paper.

The authors declare no conflict of interest.

This article is a PNAS Direct Submission.

Data deposition: Annual forest wildfire area-burned data with snow, VPD, and precipitation data and R code for accessing the file have been deposited on Topofire, https://topofire.dbs.umt.edu/public_data/helmsdeep1/fire_climate/.

[1]To whom correspondence should be addressed. Email: zaholden@fs.fed.us.

This article contains supporting information online at www.pnas.org/lookup/suppl/doi:10.1073/pnas.1802316115/-/DCSupplemental.

gridded temperature, humidity, and snow water equivalent datasets (*SI Appendix*, Figs. S1–S6), we examine the sensitivity of wildfire area burned to standardized hydrologic and precipitation indices. We then quantify trends in historical fire season (May–September) precipitation from 1979 to 2016 using gridded data and observations, and use path analysis to estimate the relative influence of snow, temperature, and summer precipitation on wildfire area burned.

Results

Decreased Snowpack (Hypothesis 1). Standardized snow anomaly metrics, including April 1 and maximum annual snow water equivalent (SWE), the number of snow-free days from March–September and the April 1 snow extent were not significantly correlated with annual western US wildfire area burned (Fig. 2; $r < 0.32$; $P > 0.10$). Further analysis of snow effects shows statistically significant correlations between one or more metrics of snow cover and wildfire area burned in six of the eight ecoregions (*SI Appendix*, Fig. S7). However, these snowpack/fire relationships were generally weak, particularly in the northwest United States where snow has previously been identified as a primary driver of increased fire activity. We found overall that the maximum SWE anomaly was the best predictor of western US burned area variations from among the suite of potential snow metrics; therefore, we

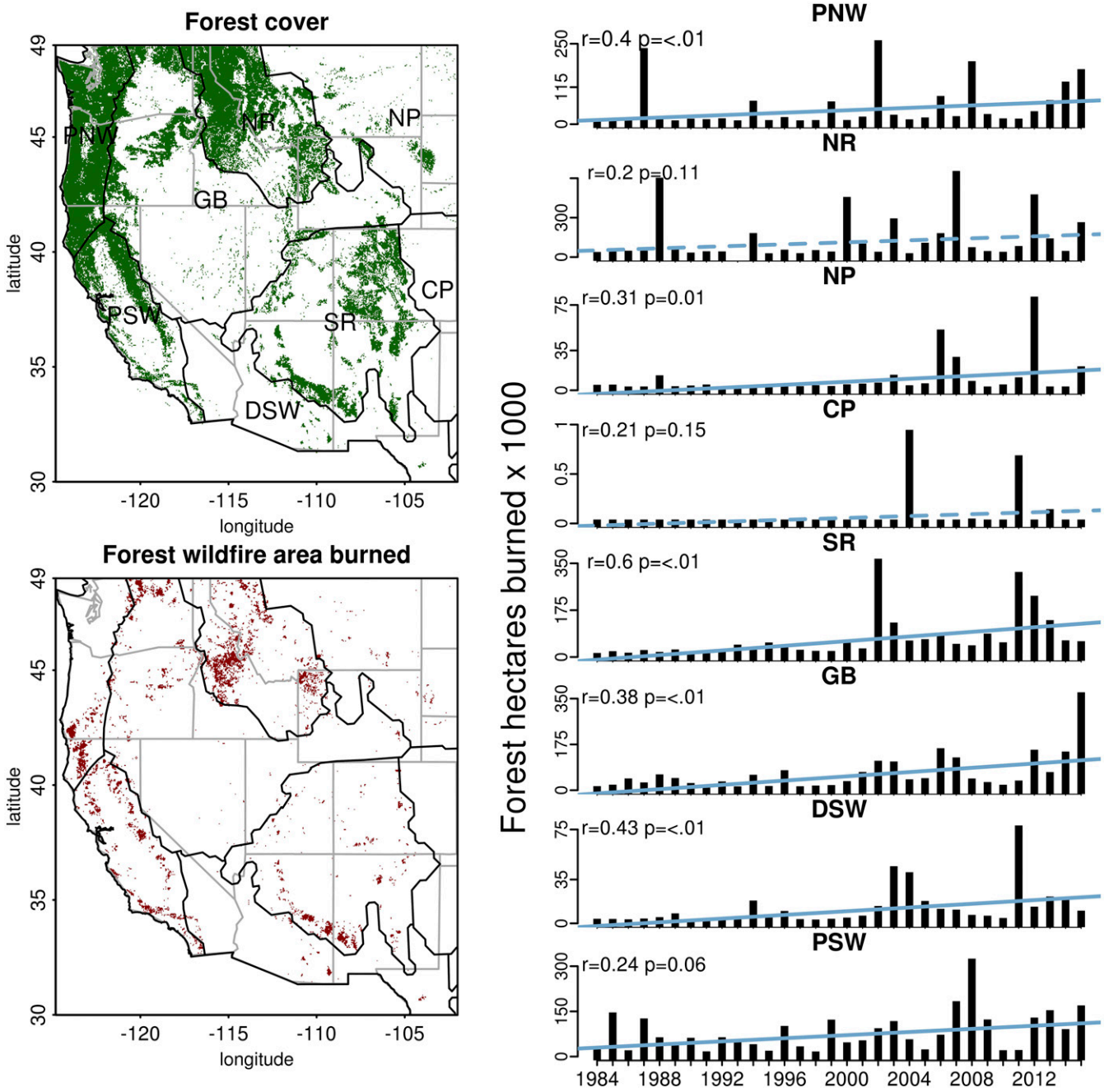

Fig. 1. Forest cover and forest wildfire area burned from 1984 to 2015 in the western United States with eight NEON domains outlined in black. (*Right*) Total annual forested hectares burned within each NEON domain. Blue lines show the linear trend in area burned, with a solid line indicating a statistically significant trend at $P < 0.10$. CP, Central Plains; DSW, Desert Southwest; GB, Great Basin; NP, Northern Plains; NR, Northern Rockies; PNW, Pacific Northwest; PSW, Pacific Southwest; SR, Southern Rockies.

use maximum annual SWE as a proxy metric for decreased snowpack for the rest of the analysis.

Increasing Temperatures (Hypothesis 2). Maximum temperature (T_{max}) anomaly variations were well correlated with both westwide and ecoregional burned area variations (Fig. 2, r = 0.25–0.74). VPD and T_{max} were highly correlated (r = 0.90); therefore, we use VPD as an integrative proxy of T_{max} variations for the remainder of analyses. Consistent with previous work (9), VPD anomalies are highly correlated to burned area variations (r = 0.21–0.82, Fig. 2), and in most ecoregions, VPD is a stronger correlate of wildfire area burned than both temperature and precipitation when considered in isolation (Fig. 2).

Decreasing Precipitation (Hypothesis 3). Using multiple gridded datasets (12–15) and observations, we detected previously unnoted, significant decreasing trends in May–September total precipitation and the number of wetting rain days (WRD; total days with precipitation greater than or equal to 2.54 mm) from 1979 to 2016 across large areas of the western United States (Fig. 3 and *SI Appendix*, Fig. S8). Trends in total May–September precipitation are negative across 82–94% of forested area in the western United States, and statistically significant in 31–35% of that area. The median decrease is −5 mm (3.7%) per decade, with maximum decreases of −77.3 mm (47%). Trends in the number of WRD show similar patterns to those for precipitation amount, with median decreases of 1 d (6%) per decade, and declines of 6 d (60%) per decade in some places. We observed negative trends in WRD across 83–98% of forested areas in the western United States, with significant declines in 36–45% of that area. Additionally, we observed increases in the mean length of continuous rain-free periods from May to September (Fig. 3). Total precipitation anomalies were strongly correlated with WRD anomalies (r = 0.95), and in all ecoregions, WRD is a better predictor of wildfire area burned than total precipitation. Therefore, WRD are used for the rest of the paper as an integrated proxy of interannual summer rainfall variations. When aggregated across the western United States for the 1984–2015 period for which wildfire data are available, decreases in fire season WRD are highly significant (Fig. 4, r = −0.46; P < 0.01) and correspond to the large increasing trends in forest wildfire area burned (Fig. 4; r = 0.83; P < 0.01).

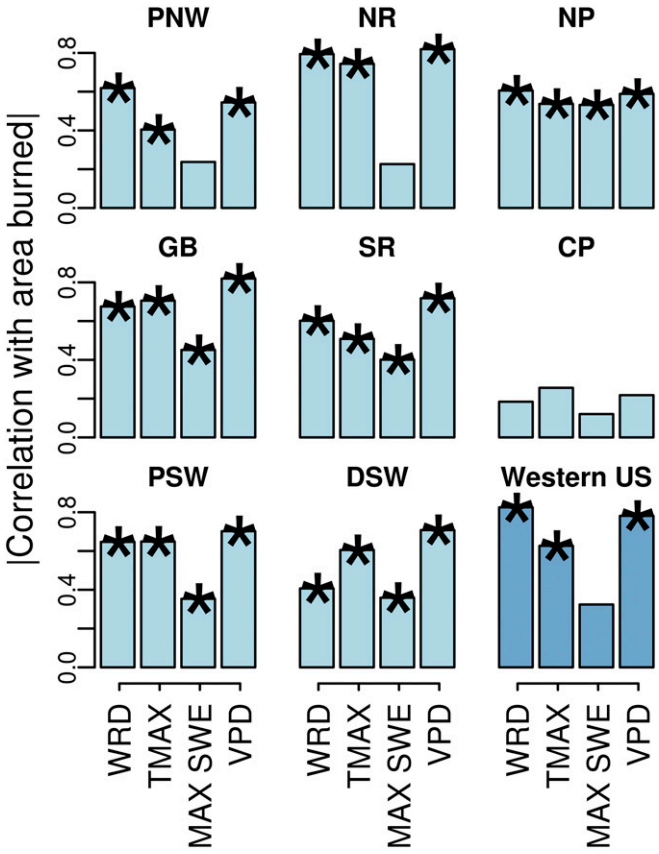

Fig. 2. Linear correlations (Pearson's r) between forest wildfire area burned (log transformed) from 1984 to 2015 and standardized May–September WRD, maximum temperature, maximum SWE, and maximum daytime VPD across eight NEON domains and for all forest areas in the western United States. An asterisk indicates statistical significance at P = 0.10. All negative values are expressed as absolute values for visual interpretation. NEON ecoregion names are identified in Fig. 1.

Precipitation, near-surface air temperature, and VPD are fundamentally related because soil moisture modulates the exchange of energy through the partitioning of latent and sensible heating. This connection is well known (16–18) and in the context of drought described as complementary (19), where onset of high evaporative demand occurs once soils begin to dry, resulting in increased sensible heating, warmer surface temperatures, and increases in atmospheric saturation vapor pressure that increase VPD, and consequently potential evapotranspiration. The downward trends in precipitation and WRD noted here occur during a season when downward radiative fluxes and evaporative demand are at their peak. In the absence of summer precipitation, soil water balance deficits accrue quickly, leading to rapid onset of drying and warming.

We find moderate to strong correlations between WRD and T_{max} and VPD (Fig. 5 and *SI Appendix*, Fig. S10), with the number of WRD during the fire season accounting for 46.2% and 72.2% of the interannual variation in T_{max} and VPD, respectively. Ultimately, near-surface moisture deficits from less frequent rainfall increase sensible heating, resulting in warmer surface air temperatures and increased evaporative demand. Thus, seasonal weather variations are tightly coupled through these feedbacks. To effectively evaluate the individual contributions of decreased snowpack, increased temperature, and decreased precipitation on western US burned area, we must decouple their individual influences by accounting for these causal interactions.

We use path analysis (20) to evaluate the relative influence of snowpack, temperature, and precipitation on wildfire area burned and to determine which of the three hypotheses best accounts for interannual variations in western US burned area. Path analysis is a form of multivariate regression that facilitates evaluation of causality among a set of correlated variables. We consider a simple model that includes all three proxies for the hypothesized drivers of wildfire area burned: SWE, VPD, and WRD (Fig. 6). In the model, maximum SWE and WRD are considered to directly influence fire, for example by wetting fuels, or limiting fire spread into snow-covered areas. In addition, both variables influence fire indirectly by mediating summer drought and consequently atmospheric demand and VPD. After accounting for the influence of precipitation on VPD, the total effect of precipitation on wildfire area burned is large (net effect = 0.81) and substantially greater than either VPD or SWE (net effect = 0.30 and 0.01, respectively; Fig. 6). Sensitivity alone is insufficient to support our claim with respect to trends, however, so we further apply the coefficients in Fig. 6 to standardized trends in WRD (−0.49 σ per decade), VPD (+0.52 σ per decade), and SWE (−0.11 σ per decade). The standardized WRD trend is similar in magnitude to that of VPD, and the WRD trend accounts for just over 2.5 times greater proportion of the trend in area burned than does VPD and 17.2 times greater than that of SWE. Even if the effect of precipitation on energy partitioning were to be ignored by removing the effect of WRD on VPD, the effect of the trend of WRD would still be 1.8 times stronger than that of VPD and 12.1 times stronger than that of SWE.

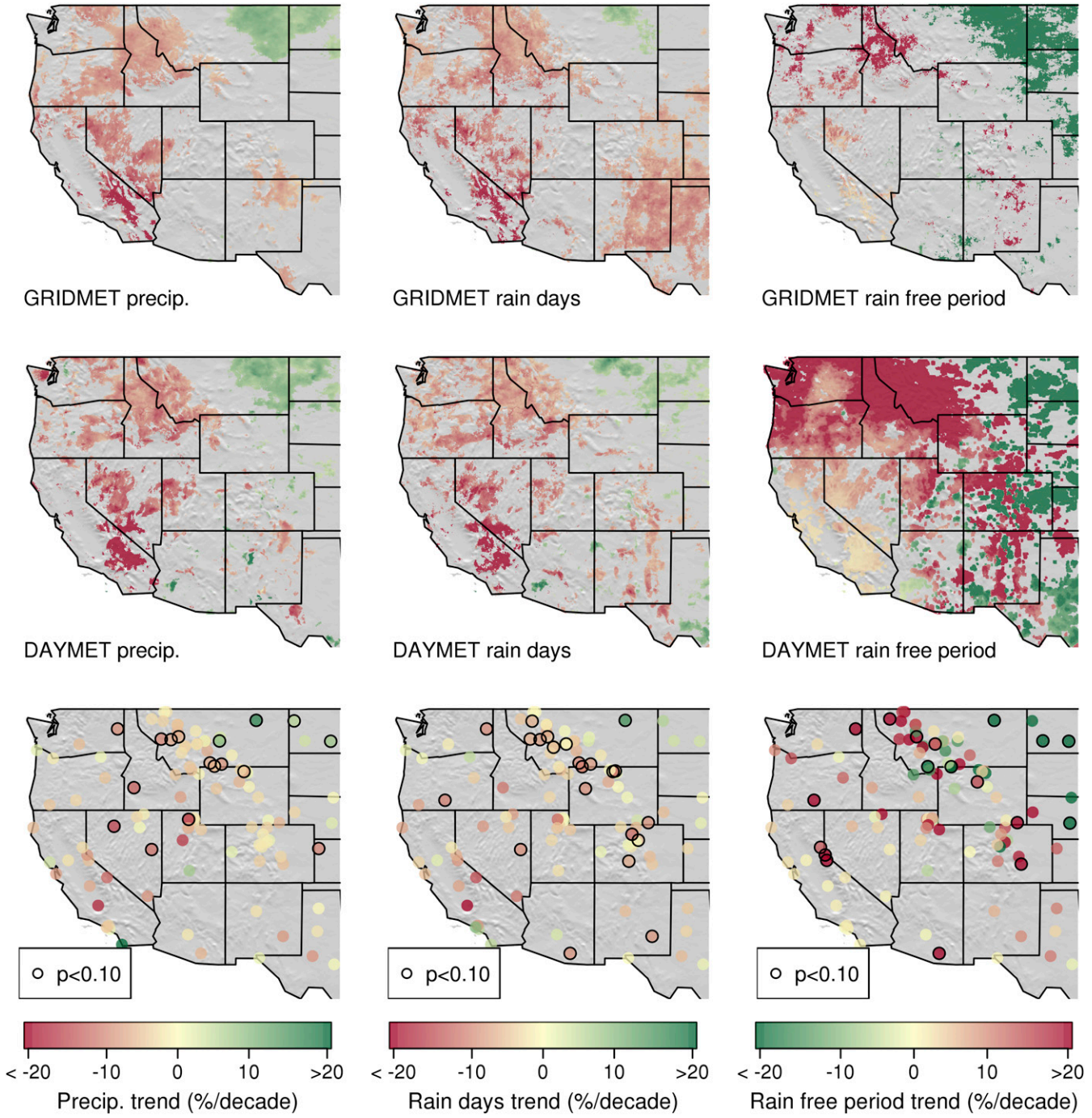

Fig. 3. Linear trends in May–September precipitation (*Left*), the number of WRD (*Center*), and the mean consecutive number of dry days (*Right*) from Daymet (1980–2016) and GRIDMET (1979–2016) datasets. Circles (*Bottom*) indicate the location of weather stations used in the trend analysis. All colored areas in gridded dataset trends and station circles outlined in black indicate statistical significance at $P = 0.10$ using a Mann–Kendall trend test.

Discussion

Without acknowledgment of the observed trends in summer precipitation, trends in recent fire activity in the West have been primarily attributed to warming temperatures, with warm winter temperatures reducing snow accumulation and lengthening the fire season (2), or through warmer summer temperatures that increase atmospheric demand that dries woody fuels (9, 11). Our findings support an additional mechanism, declining trends in summer precipitation, as a major contributor to observed trends in western US wildfire area burned during the past three decades. Looking back further in time to see if recent trends might be part of a secular trend, we used the Climate Prediction Center unified gauge-based precipitation dataset from 1948 to 2016 and found evidence of general drying in the six most western states, although with only scattered statistical significance (*SI Appendix*, Fig. S9). Given limitations of instrumentation further back in time and influence from low-frequency climate variability, other lines of evidence may be necessary to support attribution. The timing and amount of summer precipitation can influence fuel aridity through multiple pathways. In addition to directly adding moisture to woody fuels and soil, rain days are accompanied by cooler temperatures, increased humidity, and clouds that reduce

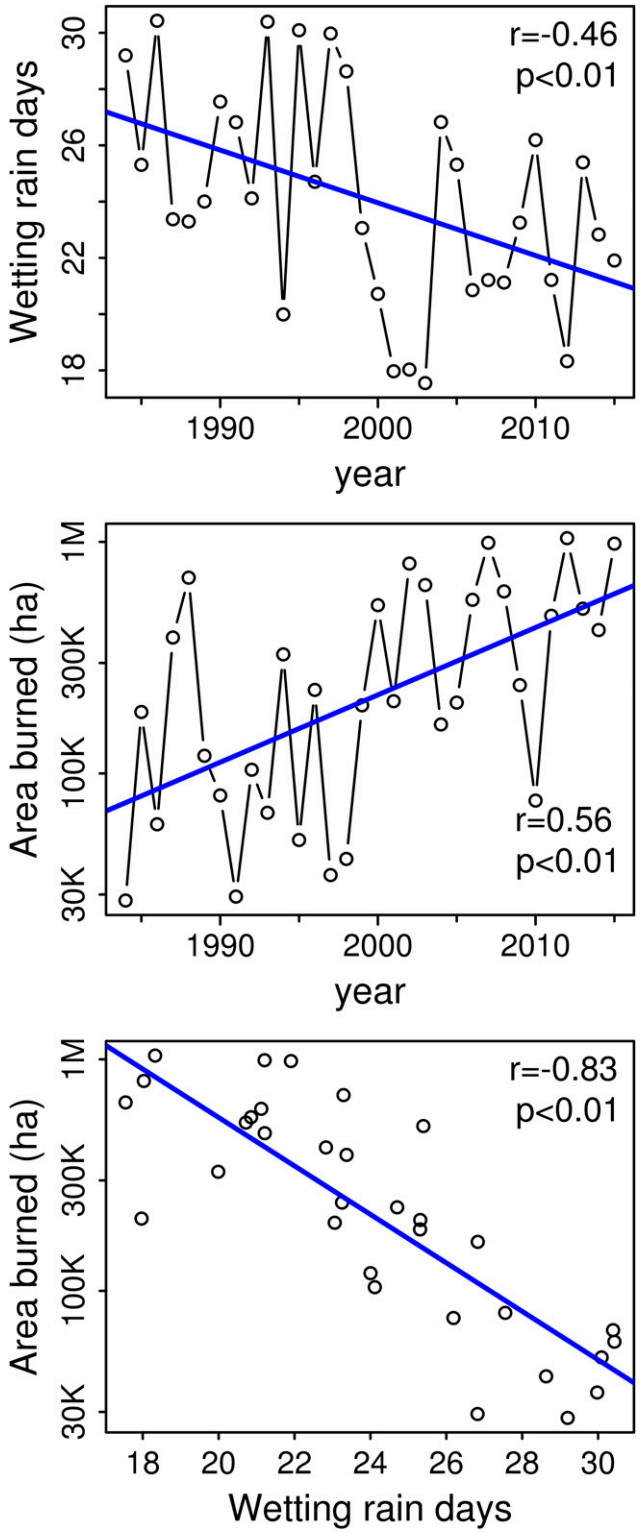

Fig. 4. Linear trends in WRD (*Top*), log-transformed wildfire area burned (*Middle*), and their correlation (*Bottom*) from 1984 to 2015 in forested areas of the western United States.

incoming radiation and consequently, near-surface heating (18). There is no doubt that regional temperature increases, independent of feedbacks from precipitation, have increased atmospheric aridity and contributed to increased wildfire activity. However, tight coupling between summer precipitation and VPD suggests that in some areas of the western United States, reductions in summer precipitation and WRD may have been the primary driver of increased wildfire activity by increasing sensible heating, resulting in warmer temperatures, higher VPD, and increased fuel aridity (Fig. 5). Additional study will be required to disentangle the regional variations in the relative influences of precipitation, temperature, and atmospheric humidity on wildland fire ecohydrology.

Climatic changes in this period of increasing fire across the West include warming temperatures in all seasons, shallower and earlier-melting snowpacks, and reduced summer precipitation in many areas. It is not surprising, then, that the frequency and size of wildfires has increased. However, contrasting multiple climatic controls show a relatively small influence from a shallow snowpack and shorter snow-covered season, but substantial influence from summer precipitation, temperature, and evaporative demand. While there is little doubt that decreasing winter snowpack can play a role in advancing fire season length, it does not appear to have been a dominant factor driving recent wildfire trends. Furthermore, both winter precipitation and temperature

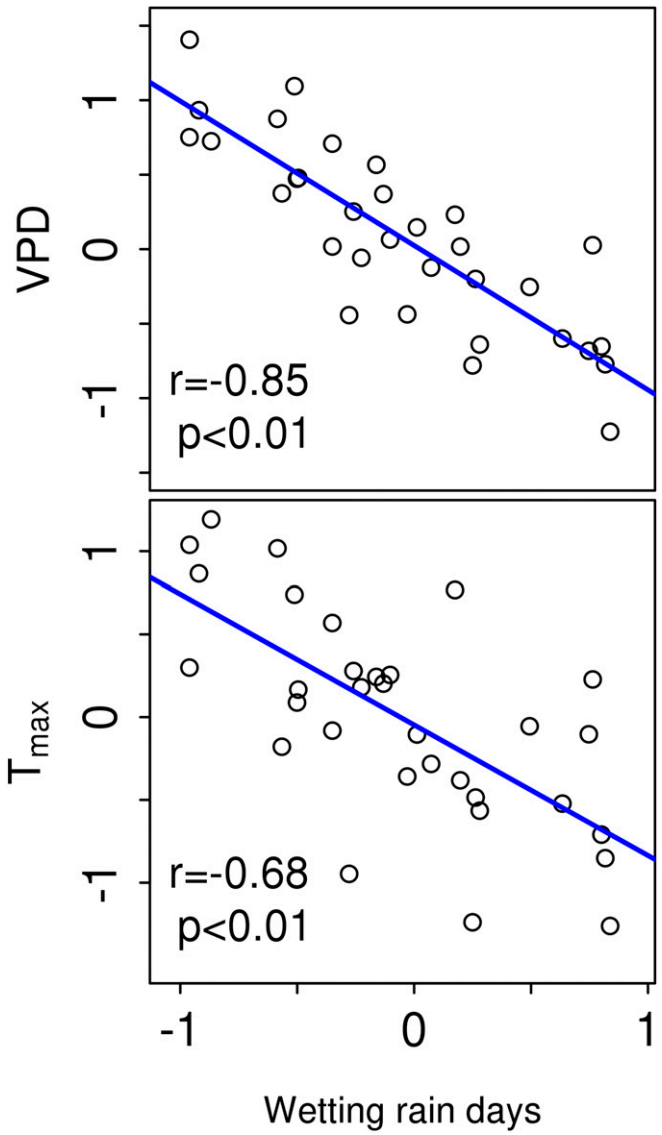

Fig. 5. May–September WRD anomalies correlated with maximum VPD and maximum temperature anomalies for western US forested areas from 1984–2015.

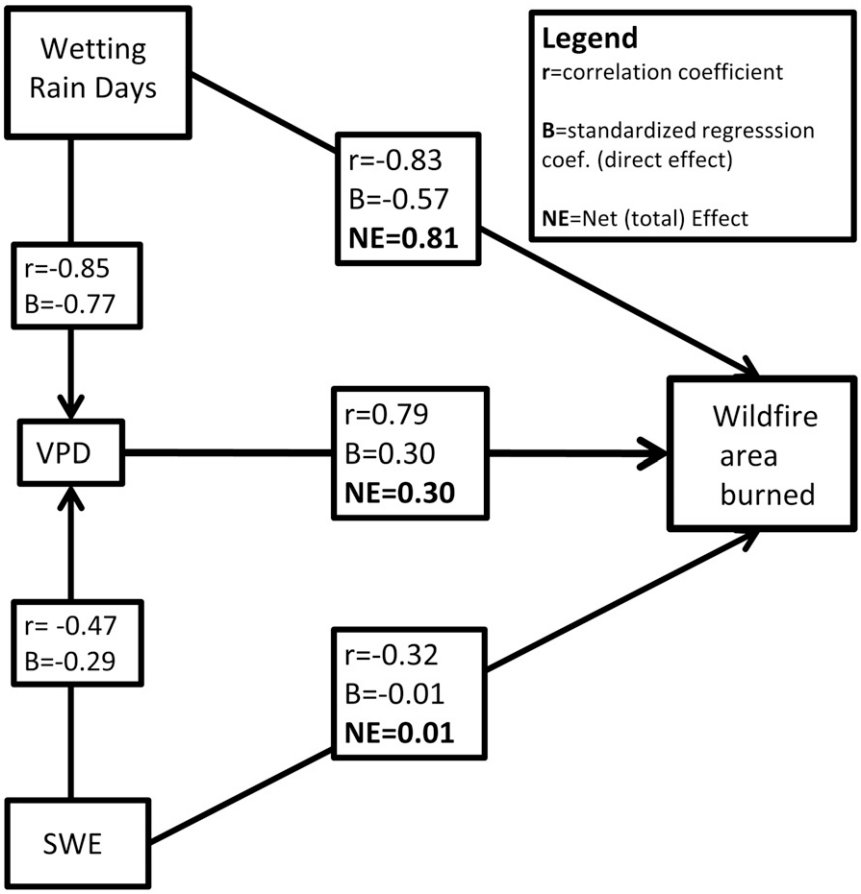

Fig. 6. Path analysis diagram illustrating relationships among precipitation, VPD, and wildfire area burned. SWE and precipitation are exogenous variables which are allowed to influence wildfire area burned directly, and indirectly as mediated by VPD.

can contribute to poor snow years and increased wildfire activity (21), with precipitation changes being more important than temperature in high-elevation interior western US mountains (22), where a large fraction of the fires have burned in the last three decades (23).

Although the sensitivity of wildfire acres burned to precipitation has been recognized (4–7), the role of precipitation in driving recent wildfire activity has been previously understated or ignored. Because precipitation responses to anthropogenic forcing are less detectable than temperature responses (24), attribution studies necessarily underestimate the relative contribution of climate change to fire through precipitation in comparison with effects through temperature (11). Indeed, although historical trends in precipitation may be substantially stronger than the climate models expected on average (11), the direction, magnitude, and spatial footprint of the observed trends are consistent with projections for the future (25, 26), making the observed decline in precipitation potentially suitable as an analog for future expectations of fire. The path analysis here illustrates that the causal connections between precipitation trends and VPD trends are an important additional consideration when forecasting future ecological responses to climatic change.

One potential mechanism for reduced summertime precipitation is the rapid decline in arctic sea ice extent (27) and subsequent weakening of zonal winds (28), which lead to slower progressions of summertime upper-level waves and promotes more prolonged midlatitude US droughts like those noted in this study. Wintertime arctic sea-ice extent has been linked to western US midsummer precipitation and temperature extrema variations and it has been suggested as one of the driving factors in burned area increases (29). The degree to which precipitation decreases noted in this study are connected to weather changes associated with shrinking arctic sea ice is unknown. Further exploration is needed to better understand the coupling between arctic sea-ice variations and midlatitude US weather.

Although we focus here primarily on wildfire activity, decreasing summer precipitation, longer intervals without rain, and associated increases in aridity have broad ecological and socioeconomic implications for other sectors of the western United States, including agriculture, forestry, and regional water demand. Drought across the United States can reduce grain yields, send ripple effects through global commodities markets, and potentially impact global food security (30). Further, warm, dry summers with high evaporative demand can reduce forest productivity in places like the Pacific Northwest (31), where timber production is a major industry. Thus, long rain-free periods and prolonged summer droughts like those experienced in the Pacific Northwest during the past decade can have serious economic consequences in addition to the costs of managing the wildfires typically associated with dry conditions.

Our ability to manage wildfires more proactively and effectively hinges to some degree on understanding and ultimately forecasting the seasonal climatic and hydrologic mechanisms that regulate them. Relatively weak regulation by more strongly predictive indicators, like winter snowpack, could further challenge wildland fire managers tasked with forecasting seasonal fire activity, and suggests that targets for seasonal outlooks may need to more strongly emphasize predictors of summer rainfall. Furthermore, the trends in summer precipitation observed here are consistent with climate change projections for the western United States in the coming decades which predict substantial decreases in summer precipitation (25, 26) and lengthening

windows without wetting rain events (32). If decreasing trends in summer precipitation continue, the result will likely be a continuing pattern of dry, warm summers that result in increasingly more severe fire seasons.

Methods

Development of Historical Daily Gridded Temperature, Humidity, and Snow Data. To address the impacts of snow cover on wildfire area burned, we developed high-resolution (250-m) gridded daily snow water equivalent datasets from 1979 to 2015. To resolve delayed melt on north-facing slopes, we developed daily topographically resolved radiation, temperature, and humidity datasets for the continental United States as inputs to the snow model using previously published methods (33). Additional details describing modifications to the temperature, humidity, and radiation modeling and their validation with independent observations are provided in the methods below.

Development of Daily Gridded Shortwave Radiation Data. We developed daily 8 arc-s (~250 m) downward shortwave radiation grids for the continental United States following methods adapted from ref. 33. Our objective in developing more finely resolved grids was to capture differences in radiation with slope and aspect so that we could better resolve the large delay in snowmelt timing on north-facing slopes. Our approach was first to generate a set of clear-sky beam and diffuse shortwave radiation grids for each calendar day (366 d) using GRASS GIS and the module r.sun (34), that are corrected for topographic shading, but assume no cloud cover. Each clear-sky grid was generated using a fixed Linke parameter and corrected for topographic shading and local slope and aspect using a 1 arc-s (30 m) Digital Elevation Model from the National Elevation Dataset (35), resampled to 8-arc-s resolution. We then used daily total downward shortwave radiation data from the North American Land Data Assimilation System (NLDAS) (36) to adjust each clear-sky grid for cloud cover. Hourly NLDAS shortwave solar radiation (SRAD) data were acquired and averaged over 24 h for each calendar day. Before deriving cloud-cover information from the NLDAS data, we used a set of historical radiation observations to correct the NLDAS grids for known biases (37, 38). In a preliminary analysis, these data were compared with station observations from the National Solar Radiation Database (NSRDB) (39), revealing systematic spatial bias with patterns similar to previously published studies (37). To correct for this bias we used principal components analysis (PCA) on a matrix of monthly mean bias for 188 NSRDB stations over the period from 1979 to 2010. Bias was expressed as the ratio between the measured and NLDAS radiation. The first three principal components were interpolated using generalized additive models with *x*, *y*, and distance to ocean as explanatory variables, which were then combined with monthly loadings to derive spatial bias correction multipliers for each month. These were then applied over all days in a given month. NSRDB data were unavailable after 2010, so a separate PCA bias correction was developed using solar radiation data from 115 Climate Reference Network (CRN) stations for the 2011–2015 period (40). The proportion of diffuse radiation was calculated from the clearness index K_c using the function from ref. 41, which was then applied to the bias-corrected NLDAS SRAD to get estimated beam and diffuse radiation at the ~10-km scale. Beam and diffuse coefficients were then calculated as the ratio between these values and their clear-sky counterparts derived from r.sun at the same resolution assuming no topography but adjusted for elevation. The beam and diffuse coefficients were then resampled to ~250-m resolution, multiplied by their respective clear-sky grids and summed to produce a final ~250-m radiation grid. The final set of daily radiation grids are adjusted for cloud cover and differences associated with slope and aspect, and show excellent agreement with surface weather station observations. *SI Appendix*, Fig. S1 shows mean seasonal bias in the 1979–2010 NLDAS SRAD relative to station observations from NSRDB. Mean absolute error (MAE) for the mean monthly uncorrected NLDAS was 15.77 W/m^2, which was reduced following bias correction to 9.62 W/m^2. *SI Appendix*, Fig. S2 shows mean seasonal bias for 2011–2015 NLDAS SRAD relative to CRN data. MAE for the mean monthly uncorrected NLDAS was 18.17 W/m^2, and after correction it was 10.57 W/m^2.

Development of Gridded Daily Temperature and Humidity Data. Daily historical (1979–2015) gridded minimum and maximum temperature and mean daily dewpoint data were created at a resolution of 250 m for the conterminous United States following methods described in ref. 33. Minor changes in the derivation of the linear regression coefficients used to correct for local terrain effects and accuracy assessment methods are described below. Grids for minimum and maximum temperature and mean daily dewpoint were developed separately, but each relies on the same basic approach. Initial air-temperature estimates are made for each day by interpolating pressure-level free-air temperature or dewpoint temperature lapse rate to a 250-m resolution digital elevation model using the Climate Forecast System Reanalysis data (42). Next, a set of previously estimated linear regression coefficients is applied to the lapse estimated temperature grids to adjust for local effects of solar insolation and surface soil moisture. Finally, residual errors in the grids are identified using a subset of available permanent weather station observations that include Snowpack Telemetry stations (SnoTel), Remote Automated Weather Stations, and the Global Historical Climatology Network (GHCN-D, ref. 43). This error is estimated using thin-plate spline regression, with the fitted model then used to adjust the gridded temperature predictions, ensuring the final gridded product generally matches measured near-surface temperature or humidity. In expanding our data to encompass the continental United States, proximity to large coastal areas had to be accounted for. Therefore, we included an estimate of distance to coast (log transformed) as an independent variable in our thin-plate spline regression models in addition to *x* and *y*.

Linear model coefficients for local minimum and maximum temperature effects were estimated using 1 million randomly sampled temperature observations including 500,000 quality assured and homogenized observations from ref. 44 and a network of low-cost temperature measurement devices (45) expanded to include an additional 244 sensors distributed across the state of Washington from September 2013 to October 2014. Observations used in the estimation of linear terms for the model of daily mean dewpoint temperature included most weather station networks in the United States, including Remote Automated Weather Stations, Integrated Surface Data, and historical observations from the Meteorological Data Assimilation System. Additionally, we included humidity observations collected at 222 of the low-cost temperature monitoring sites in Washington, Idaho, and Montana.

For maximum daily temperature, we considered a set of candidate models that included solar radiation, modeled soil moisture, canopy cover from the Moderate Resolution Imaging Spectroradiometer (MODIS) Vegetation Continuous Fields product (46), and their interactions. Development of the daily soil moisture model is described in further detail below. For daily minimum temperature, variables included in model selection included a static physiographic map of potential for cold air drainage potential expanded to the continental United States (33), standardized geopotential height, daily mean relative humidity, and their interactions. Candidate variables for the mean daily dewpoint model included daily soil moisture, total daily solar radiation, and minimum daily temperature. Model selection was performed using an independent set of 25% of withheld data. The selected model for maximum temperature contained linear terms for soil moisture, solar radiation, and canopy cover with no interaction terms. Because MODIS canopy cover data are unavailable before 2000, canopy cover was set as the 2015 value, eliminating any dynamic variation in temperature associated with canopy cover through time.

We assessed the overall accuracy of the final temperature and humidity models using a 10-fold cross-validation. For each iteration, we withheld 10% of the observations for validation and used the remaining observations for response surface estimation. Each model was applied daily (including estimation of the daily error offset) using the training stations, only over the full time period, to collect a full error history at each of the withheld test stations. Model accuracy is reported as the MAE between model predictions and withheld data at each station. *SI Appendix*, Fig. S3 shows maximum temperature model error mean by US climate division and season. The overall MAE for the maximum temperature model across the conterminous United States was 1.13 °C and 1.17 °C for the western US study domain. *SI Appendix*, Fig. S4 shows minimum temperature model error mean by US climate division and season. The overall MAE for the minimum daily temperature model was 1.42 °C across the conterminous United States and 1.57 °C for western US study domain. *SI Appendix*, Fig. S5 shows mean daily dewpoint model error by US climate division and season. The overall MAE for the mean daily dewpoint model was 1.12 °C for the conterminous United States and 1.22 °C for western US study domain.

Daily Snow Model. Daily 8-arc-s gridded SWE maps were developed for the 1979–2015 period using an empirical temperature index snow model adapted from ref. 47. Temperature index models often outperform more complex energy balance models in catchment-scale studies, but may fail to resolve topographic variations in melt associated with slope and aspect (48). To address this shortcoming, we substitute the sine coefficient used in the original model with modeled net daily shortwave radiation data extracted from the gridded dataset described above. We then calibrated the model using data from 682 Snowpack Telemetry stations and 3 y of data from each station. Model calibration was performed using the Optim function in the software environment R (R project 2010). We then evaluated the model

using 16 y of SWE observations from 819 western US SNOTEL stations. We compared modeled and observed SWE at each site using a Nashe-Sutcliffe efficiency statistic (NSE). In addition, we compared the observed and predicted date of snow departure for each year at each station. Accuracy statistics for both evaluations are shown in *SI Appendix*, Fig. S6. Modeled SWE and snow-free days show strong agreement with observations. The average NSE statistic across all stations was 0.87 and the MAE for the estimate of number of snow-free days was 8.6 d. Four metrics were derived from the daily data and used as indicators of snow volume and melt timing: April 1 SWE, maximum SWE, the number of snow-free days from March 1–September 30, and snow-covered area on April 1. All indices were converted to standardized anomalies relative to the 1981–2010 mean and SD.

Wildfire area-burned data. We used data from the monitoring trends in burn severity project [MTBS, (49)] to estimate total annual forested area burned in six western US ecoregions from 1984 to 2015. Fires classified as prescribed burns by MTBS were excluded. We defined forested areas using a forest cover mask developed using the MODIS 250-m resolution continuous fields (VCF) data (46). Each 8-d MODIS VCF grid from 2000 to 2015 was classified as forested where any pixel had canopy cover values greater than 10%. Then, a final mask was created, where any cell with forest cover during the full image time series was classified as forest and then resampled to 30-m resolution. Area-burned estimates were extracted on a per-fire basis and summed by year across the western US and within eight western US ecoregions from the National Ecological Observatory Network.

Wildfire area-burned predictors. Monthly mean maximum VPD was estimated from monthly mean dewpoint temperature and monthly mean maximum temperature using the gridded datasets described above. The monthly mean maximum saturation vapor pressure (e_s) was first calculated from mean monthly maximum temperature grids. Monthly mean maximum actual vapor pressure (e_a) was then estimated using dewpoint temperature. The VPD was then calculated as e_s minus e_a. Temperature, VPD, and snow datasets were extracted from within western US forested areas with the bounding extent defined by eight western US National Ecological Observatory Network (NEON) domains, after resampling the forest cover mask to 30-m resolution. The extractions and anomaly calculations were performed twice, first using all western US forests, and then separately from within each NEON domain. Precipitation and WRD anomalies (number of days with ≥2.54 mm of precipitation) were extracted using data from ref. 14. We included four snow metrics in our analysis: April 1 SWE, Maximum SWE from January 1–June 30, the number of snow-free days from March 1–September 30, and snow cover extent on April 1 of each year. All metrics were converted to standardized anomalies (z scores) relative to the 1981–2010 average and SD. Here, the z score was first calculated for each forested grid cell. The grid-cell anomalies were then averaged across each domain. Annual forest wildfire area-burned data with snow, VPD, and precipitation data and R code for accessing the file can be downloaded at https://topofire.dbs.umt.edu/public_data/helmsdeep1/fire_climate/.

Precipitation Trend Tests. We calculated trends in May–September total precipitation and number of WRD using data from multiple gridded datasets and surface weather observations (Fig. 3). Precipitation trends were calculated using 1980–2016 1-km resolution Daymet (13), and 1979–2016 4-km resolution GRIDMET data (14). Surface observations for precipitation trends included 55 Snowpack Telemetry Stations and 53 GHCN-D stations. Trends were calculated using the Mann–Kendall trend test and evaluated at a significance level of $P < 0.10$. Both gridded datasets rely on surface observations, with Daymet data estimating precipitation by directly interpolating the observations, and GRIDMET by bias-correcting NLDAS-2 data at a monthly time step using grids derived from interpolated observations. We tested for trends in May–September total precipitation and WRD using two reanalysis datasets (*SI Appendix*, Fig. S8); the North American Regional Reanalysis (NARR, ref. 12) and the ERA-interim reanalysis (15). The NARR assimilates some surface weather observations, while the ERA-interim does not. Additionally, we examined trends in the Climate Prediction Center unified gauge-based precipitation dataset from 1948 to 2016 (*SI Appendix*, Fig. S9).

ACKNOWLEDGMENTS. We thank Erin Landguth and the Computational Ecology Laboratory for supporting this project. This work was supported by the National Aeronautics and Space Administration applied science program under Award NNH11ZDA001N-FIRES.

1. Westerling AL, Hidalgo HG, Cayan DR, Swetnam TW (2006) Warming and earlier spring increase western U.S. forest wildfire activity. *Science* 313:940–943.
2. Westerling AL, Gershunov A, Brown TJ, Cayan DR, Dettinger MD (2003) Climate and wildfire in the western United States. *Bull Am Meteorol Soc* 84:595–604.
3. Westerling AL, Turner MG, Smithwick EAH, Romme WH, Ryan MG (2011) Continued warming could transform Greater Yellowstone fire regimes by mid-21st century. *Proc Natl Acad Sci USA* 108:13165–13170.
4. Holden ZA, Morgan P, Crimmins MA, Steinhorst RK, Smith AMS (2007) Fire season precipitation variability influences fire extent and severity in a large southwestern wilderness area, United States. *Geophys Res Lett* 34:L16708.
5. Littell JS, McKenzie D, Peterson DL, Westerling AL (2009) Climate and wildfire area burned in western U.S. ecoprovinces, 1916-2003. *Ecol Appl* 19:1003–1021.
6. Jolly WM, et al. (2015) Climate-induced variations in global wildfire danger from 1979 to 2013. *Nat Commun* 6:7537.
7. Abatzoglou JT, Kolden CA (2013) Relationships between climate and macroscale area burned in the western United States. *Int J Wildland Fire* 22:1003–1020.
8. Williams AP, et al. (2014) Causes and implications of extreme atmospheric moisture demand during the record-breaking 2011 wildfire season in the southwestern United States. *J Appl Meteorol Climatol* 53:2671–2684.
9. Williams AP, et al. (2013) Temperature as a potent driver of regional forest drought stress and tree mortality. *Nat Clim Chang* 3:292–297.
10. Williams AP, et al. (2015) Correlations between components of the water balance and burned area reveal new insights for predicting forest fire area in the southwest United States. *Int J Wildland Fire* 24:14–26.
11. Abatzoglou JT, Williams AP (2016) Impact of anthropogenic climate change on wildfire across western US forests. *Proc Natl Acad Sci USA* 113:11770–11775.
12. Mesinger F, et al. (2006) North American regional reanalysis. *Bull Am Meteorol Soc* 87: 343–360.
13. Thornton PE, et al. (2017) Daymet: Daily Surface Weather Data on a 1-km Grid for North America (ORNL DAAC, Oak Ridge, TN), Version 3.
14. Abatzoglou JT (2011) Development of gridded surface meteorological data for ecological applications and modelling. *Int J Climatol* 33:121–131.
15. Dee P, et al. (2011) The ERA-Interim reanalysis: Configuration and performance of the data assimilation system. *Q J R Meteorol Soc* 137:553–597.
16. Berg A, et al. (2015) Interannual coupling between summertime surface temperature and precipitation over land: Processes and implications for climate change. *J Clim* 28: 1308–1328.
17. Yin D, Roderick ML, Leech G, Sun F, Huang Y (2014) The contribution of reduction in evaporative cooling to higher surface air temperatures during drought. *Geophys Res Lett* 41:7891–7897.
18. Trenberth KE, Shea DJ (2005) Relationships between precipitation and surface temperature. *Geophys Res Lett* 32:L14703.
19. Bouchet RJ (1963) Evapotranspiration réelle et potentielle, signification climatique. *Proceedings of the IASH General Assembly* 62:134–142.
20. Wright S (1934) The method of path coefficients. *Ann Math Stat* 5:161–215.
21. Holden ZA, Luce CH, Crimmins MA, Morgan P (2012) Wildfire extent and severity correlated with annual streamflow distribution and timing in the Pacific Northwest, USA (1984–2005). *Ecohydrology* 5:677–684.
22. Luce CH, Lopez-Burgos V, Holden Z (2014) Sensitivity of snowpack storage to precipitation and temperature using spatial and temporal analog models. *Water Resour Res* 50:9447–9462.
23. Dillon GK, et al. (2011) Both topography and climate affected forest and woodland burn severity in two regions of the western US, 1984 to 2006. *Ecosphere* 2:art130.
24. Deser C, Phillips A, Bourdette V, Teng H (2012) Uncertainty in climate change projections: The role of internal variability. *Clim Dyn* 38:527–546.
25. Rupp DE, Abatzoglou JT, Mote PW (2017) Projections of 21st century climate of the Columbia River Basin. *Clim Dyn* 49:1783–1799.
26. Rupp DE, et al. (2017) Seasonal spatial patterns of projected anthropogenic warming in complex terrain: A modeling study of the western US. *Clim Dyn* 48:2191–2213.
27. Stroeve JC, et al. (2012) The Arctic's rapidly shrinking sea ice cover: A research synthesis. *Clim Change* 110:1005–1027.
28. Francis JA, Vavrus SJ (2012) Evidence linking Arctic amplification to extreme weather in mid-latitudes. *Geophys Res Lett* 39:L06801.
29. Knapp AP, Soulé TP (2017) Spatio-temporal linkages between declining Arctic sea-ice extent and increasing wildfire activity in the western United States. *Forests* 8:313.
30. Boyer JS, et al. (2013) The U.S. drought of 2012 in perspective: A call to action. *Glob Food Secur* 2:139–143.
31. Waring RH, Franklin JF (1979) Evergreen coniferous forests of the Pacific Northwest. *Science* 204:1380–1386.
32. USGCRP (2017) *Climate Science Special Report: Fourth National Climate Assessment*, eds Wuebbles DJ, et al. (US Global Change Research Program, Washington, DC), Vol 1.
33. Holden ZA, et al. (2016) Development of high-resolution (250 m) historical daily gridded air temperature data using reanalysis and distributed sensor networks for the US Northern Rocky Mountains. *Int J Climatol* 36:3620–3632.
34. Hofierka J, Suri M (2004) A new GIS-based solar radiation model and its application to photovoltaic assessments. *Trans GIS* 8:175–190.
35. Gesch DB (2007) The national elevation dataset. *Digital Elevation Model Technologies and Applications—The DEM Users Manual*, ed Maune D (American Society for Photogrammetry and Remote Sensing, Bethesda), pp 99–118.
36. Mitchell KE, et al. (2004) The multi-institution North American Land Data Assimilation System (NLDAS): Utilizing multiple GCIP products and partners in a continental distributed hydrological modeling system. *J Geophys Res* 109:D07S90.
37. Lewis CS, Geli HME, Neale CMU (2014) Comparison of the NLDAS weather forcing model to agrometeorological measurements in the western United States. *J Hydrol (Amst)* 510:385–392.

38. Luo L, et al. (2003) Validation of the North American Land Data Assimilation System (NLDAS) retrospective forcing over the southern Great Plains. *J Geophys Res* 108:8843.
39. Wilcox S (2012) National Solar Radiation Database 1991–2010 Update: User's Manual. NREL/TP-5500-54824 (National Renewable Energy Laboratory, Golden, CO).
40. Diamond HJ, et al. (2013) U.S. climate reference network after one decade of operations: Status and assessment. *Bull Am Meteorol Soc* 94:485–498.
41. Erbs DG, Klein SA, Duffie JA (1982) Estimation of the diffuse radiation fraction for hourly, daily and monthly-average global radiation. *Sol Energy* 28:293–302.
42. Saha S, et al. (2010) The NCEP climate forecast system reanalysis. *Bull Am Meteorol Soc* 91:1015–1057.
43. Menne MJ, Durre I, Vose RS, Gleason BE, Houston TG (2012) An overview of the global historical climatology network-daily database. *J Atmos Ocean Technol* 29:897–910.
44. Oyler JW, Ballantyne A, Jencso K, Sweet M, Running SW (2014) Creating a topoclimatic daily air temperature dataset for the conterminous United States using homogenized station data and remotely sensed land skin temperature. *Int J Climatol* 35: 2258–2279.
45. Holden ZA, Klene AE, Keefe RF, Moisen GG (2013) Design and evaluation of an inexpensive radiation shield for monitoring surface air temperatures. *Agric For Meteorol* 180:281–286.
46. Carroll M, et al. (2011) MODIS vegetative cover conversion and vegetation continuous fields BT. *Land Remote Sensing and Global Environmental Change: NASA's Earth Observing System and the Science of ASTER and MODIS*, eds Ramachandran B, Justice CO, Abrams MJ (Springer, New York), pp 725–745.
47. Fontaine TA, Cruickshank TS, Arnold JG, Hotchkiss RH (2002) Development of a snowfall-snowmelt routine for mountainous terrain for the Soil Water Assessment Tool (SWAT). *J Hydrol (Amst)* 262:209–223.
48. Hock R (2003) Temperature index melt modelling in mountain areas. *J Hydrol (Amst)* 282:104–115.
49. Eidenshink JC, et al. (2007) A project for monitoring trends in burn severity. *Fire Ecol* 3:3–21.